J Pharmacokinet Pharmacodyn (2012) 39:643–659
DOI 10.1007/s10928-012-9276-y

ORIGINAL PAPER

Bench to bedside translation of antibody drug conjugates using a multiscale mechanistic PK/PD model: a case study with brentuximab-vedotin

Dhaval K. Shah · Nahor Haddish-Berhane · Alison Betts

Received: 18 July 2012 / Accepted: 19 October 2012 / Published online: 15 November 2012
© Springer Science+Business Media New York 2012

Abstract To build a multiscale mechanism based pharmacokinetic–pharmacodynamic (PK/PD) model for antibody drug conjugates (ADCs), using brentuximab-vedotin as an example, for preclinical to clinical translation of ADC efficacy. Brentuximab-vedotin experimental data, collected from diverse publications, were employed in the following steps to build and validate the model: (1) characterization of ADC and payload PK at the cellular level, (2) characterization of payload PK in plasma and tumor tissue of xenograft mouse, (3) characterization of ADC PK in mouse plasma, (4) prediction of the tumor payload concentrations in xenograft mouse by integrating parameters obtained from steps 1–3 with the novel tumor disposition model for ADC, (5) characterization of preclinical brentuximab-vedotin tumor growth inhibition data using the novel PK/PD model, (6) characterization of ADC and payload PK in cancer patients, and (7) prediction of clinical responses of brentuximab-vedotin using the PK/PD model, by integrating PK parameters obtained from step 6, and translated mouse parameters from step 5; and comparing them with clinical trial results. The tumor disposition model was able to accurately predict xenograft tumor and plasma payload concentrations. PK/PD model predicted progression free survival rates and complete response rates for brentuximab-vedotin in patients were comparable to the observed clinical results. It is essential to understand and characterize the disposition of ADC and payload, at the cellular and physiological level, to predict the clinical outcome of ADC. A first of its kind mechanistic model has been developed for ADCs, which can integrate preclinical biomeasures and PK/PD data, to predict clinical response.

Keywords Antibody drug conjugate · Clinical translation · Mechanistic mathematical model · Pharmacokinetics–pharmacodynamics · Brentuximab-vedotin · SGN-35

Introduction

Antibody drug conjugates (ADC) are an upcoming anticancer modality which exploit the targeting capabilities of antibodies and potent cytotoxicity of chemicals (payload) to achieve an enhanced therapeutic index [1]. An ADC has three components: (i) antibody, responsible for the tumor specific localization of the ADC (ii) linker, responsible for specifically releasing the payload inside the tumor cell, and (iii) payload, responsible for killing the tumor cell [2]. Considering there are three different components responsible for the tumor targeting of ADCs, and delivery of their payload to the cancer cells, it becomes imperative to understand and characterize the biodisposition of each of these three components to achieve an optimized drug with maximum therapeutic potential. However, it is difficult to fully comprehend and integrate the complex, nonlinear, and many times unintuitive processes involved in the cellular and physiological disposition of ADCs and their components, without the use of a multiscale, mechanism based mathematical model. Aside from characterizing the underlying system, properly developed PK/PD models are

Electronic supplementary material The online version of this article (doi:10.1007/s10928-012-9276-y) contains supplementary material, which is available to authorized users.

D. K. Shah (✉) · N. Haddish-Berhane · A. Betts
Translational Research Group, Department of Pharmacokinetics Dynamics and Metabolism, Pfizer Global Research and Development, Groton Labs, MS 8220-4573, Eastern Point Road, Groton, CT 06340, USA
e-mail: Dhavalkumar.K.Shah@pfizer.com

also capable of guiding the dose regimen optimization, and translating preclinical data to the clinic [3]. In order to accomplish such a comprehensive mathematical model for ADCs, we are presenting for the first time a multiscale mechanism based PK/PD model, not only characterizing the biodisposition of ADC and payload at the cellular and physiological level, but also capable of providing translation of preclinical efficacy data to the clinic.

The model has been developed in a step-by-step manner using literature derived experimental and clinical data for brentuximab-vedotin (cAC10-vc-MMAE, SGN-35), which is being marketed for the treatment of Hodgkin's lymphoma (HL) and anaplastic large cell lymphoma (ALCL). Brentuximab-vedotin consists of an anti-CD30 antibody (cAC10) attached to potent tubulin polymerization inhibiting payload Monomethyl Auristatin E (MMAE), via a protease-sensitive dipeptide linker valine-citrulline (vc), using the conventional thiol based conjugation method [4]. The linker is specifically designed to release MMAE by lysosomal cathepsin-B cleavage in target cancer cells, while maintaining stable linkage in the systemic circulation [5]. The first step of the model building process includes validation of literature derived CD30+ cell biomeasures [6] (e.g. receptor numbers, binding affinity, internalization rate), and cellular PK parameters of brentuximab-vedotin and MMAE, by comparing predictions from a mass balance model with the results from published in vitro experiment. In the second step, a PK model for MMAE is developed by its fitting to plasma and tumor PK in a xenograft mouse, obtained after systemic MMAE administration. The next step involves developing a model to characterize the plasma PK of brentuximab-vedotin in mouse, and characterization of the average drug antibody ratio (DAR) versus time profile for brentuximab-vedotin in mouse. The fourth step integrates all the parameter values obtained from the first three steps using a novel and clinically translatable tumor disposition model, to predict tumor MMAE, unconjugated plasma MMAE, and conjugated plasma MMAE concentrations in a xenograft mouse, after systemic brentuximab-vedotin administration. Efficacy of brentuximab-vedotin in two different xenograft mouse models is characterized in the fifth step, where the predicted tumor concentrations of MMAE are correlated with tumor volumes using a semi-mechanistic model [7], to estimate the PD parameters associated with the drug. In the sixth step, PK profiles of brentuximab-vedotin and MMAE in cancer patients, obtained from two different clinical trials employing different dosing regimen, were characterized to obtain clinical PK parameters for both the molecules. Lastly, the final step deals with the preclinical to clinical translation of brentuximab-vedotin efficacy. Literature derived clinical tumor growth rates, CD30 receptor numbers, and clinical PK parameters for brentuximab-vedotin and MMAE are substituted in the preclinical PK-PD model. The model is then used to simulate clinical trials and predict objective response rates (ORR) and progression free survival rates (PFS) of patients treated with two different dosing regimen for brentuximab-vedotin. Results from simulated clinical trials are compared with the observed clinical trial results, to validate the preclinical to clinical translation ability of the proposed model.

Model development

Modeling the PK of brentuximab-vedotin and MMAE at cellular level (step-1)

In order to characterize the fate of brentuximab-vedotin and MMAE at a cellular level, a simple mass balance model was developed to mimic incubation of brentuximab-vedotin in an in vitro cell culture system, equations for which are shown below:

$$\frac{dADC_{Extra\_Cellular}}{dt} = -k_{on_{Antigen}}^{ADC} \cdot ADC_{Extra\_Cellular} \cdot (Ag_{Total} - ADC\_Ag_{Bound}) + k_{off_{Antigen}}^{ADC} \cdot ADC\_Ag_{Bound}; \quad IC = ADC^{0}_{Extra\_Cellular} \tag{1}$$

$$\frac{dADC\_Ag_{Bound}}{dt} = k_{on_{Antigen}}^{ADC} \cdot ADC_{Extra\_Cellular} \cdot (Ag_{Total} - ADC\_Ag_{Bound}) - k_{off_{Antigen}}^{ADC} \cdot DC\_Ag_{Bound} - k_{int_{Ag}} \cdot ADC\_Ag_{Bound}; \; IC = 0 \tag{2}$$

$$\frac{dPL_{Intra\_Cellular}}{dt} = k_{int_{Ag}} \cdot ADC\_Ag_{Bound} \cdot DAR - k_{out_{PL}} \cdot PL_{Intra\_Cellular}; \; IC = 0 \tag{3}$$

$$\frac{dPL_{Extra\_Cellular}}{dt} = k_{out_{PL}} \cdot PL_{Intra\_Cellular}; \; IC = 0 \tag{4}$$

where $ADC_{Extra\_Cellular}$ is concentration of extracellular ADC, ADC_Ag_{Bound} is concentration of tumor antigen bound ADC on cell surface, $PL_{Intra\_Cellular}$ is concentration of intracellular payload, and $PL_{Extra\_Cellular}$ is concentration of extracellular payload. Due to the lack of sufficient information to estimate relevant parameters at this early in vitro stage, it was assumed that the ADC is stable in the cell culture medium [8], and there is a negligible uptake of released unconjugated payload from media to the cell. Please refer to the glossary in Table 1 for detailed explanation of all the symbols used in aforementioned and all other equations in this manuscript.

Table 1 A glossary of the terms used in model equations

Symbol	Definition	Unit
$ADC_{Extra\_Cellular}$	Brentuximab-vedotin concentration in cell culture media	nM
$k_{on}^{ADC}{}_{Antigen}$, $k_{off}^{ADC}{}_{Antigen}$	Association, and dissociation, rate constants between brentuximab-vedotin and CD30	1/nM/day, 1/day
Ag_{Total}, ADC_Ag_{Bound}	Total CD30, and brentuximab-vedotin bound CD30, concentrations	nM
$PL_{Intra\_Cellular}$, $PL_{Extra\_Cellular}$	MMAE concentrations inside the cells, and in the cell culture media	nM
$k_{int_{Ag}}$	Internalization rate of CD30 inside the cell	1/day
$k_{out_{PL}}$	Efflux rate of MMAE from the cell	1/day
DAR	Drug antibody ratio i.e. #payload(s)/antibody	Unitless
$X1_{PL}$, $X2_{PL}$	Amount of MMAE in central, and peripheral, compartment	Nanomole
CL_{PL}, CLD_{PL}	Plasma clearance, and distribution clearance, of MMAE	L/day/Kg
$V1_{PL}$, $V2_{PL}$	MMAE volume of distribution for central, and peripheral, compartment	L/Kg
P_{PL}, D_{PL}	The rate of permeability, and diffusion, of MMAE across the tumor blood vessels	μm/day, cm^2/day
R_{Cap}, R_{Krogh}	Radius of tumor blood capillary, and an average distance between two capillaries	μm
ε_{PL}	Tumor void volume for MMAE	Unitless
R_{Tumor}	Radius of the tumor	cm
$PL^{Tumor}_{Intra\_Cellular}$, $PL^{Tumor}_{Extra\_Cellular}$	MMAE concentration inside tumor cells, and in tumor extracellular space	nM
$k_{int_{PL}}$	MMAE nonspecific uptake rate in cancer cell	1/day
$k_{on}^{PL}{}_{Tubulin}$, $k_{off}^{PL}{}_{Tubulin}$	Association, and dissociation, rate constants between MMAE and unknown cell component	1/nM/day, 1/day
$Tubulin_{Total}$	Total concentration of MMAE binding intracellular component	nM
$PL^{Bound}_{Tubulin}$	Concentration of MMAE bound inside the cell	nM
k_{dis}	Dissociation rate of MMAE from brentuximab-vedotin	1/day
$X1_{ADC}$, $X2_{ADC}$	Amount of brentuximab-vedotin in central, and peripheral, compartment	Nanomole
CL_{ADC}, CLD_{ADC}	Plasma clearance, and distribution clearance, of brentuximab-vedotin	L/day/Kg
$V1_{ADC}$, $V2_{ADC}$	Brentuximab-vedotin volume of distribution for central, and peripheral, compartment	L/Kg
P_{ADC}, D_{ADC}	The rate of permeability, and diffusion, of brentuximab-vedotin across the tumor blood vessels	μm/day, cm^2/day
ε_{ADC}	Tumor void volume for brentuximab-vedotin	Unitless
$ADC^{Free}_{Tumor\_ExtraCellular}$, $ADC^{Bound}_{Tumor\_ExtraCellular}$	Free, and CD30 bound, brentuximab-vedotin concentrations in tumor extracellular space	nM
$C1_{PL}$, $C2_{PL}$	Concentrations of MMAE in central, and peripheral, compartment	nM
$V1$, $V2$, $V3$, $V4$	Tumor volume in the growth, and three transduction, compartment	mm^3
$V1_{Initial}$, TV, V_{Max}	Initial tumor volume, Total tumor volume, and maximum possible tumor volume	mm^3
$k_{g_{Exponenial}}$, $k_{g_{Linear}}$, $\omega k_{g_{Exponenial}}$, $\omega k_{g_{Linear}}$	Exponential and linear growth rates for tumor, and inter-individual variability associated with them	1/day, mm^3/day
$k_{kill_{Max}}$, $\omega k_{kill_{Max}}$	Maximum killing rate constant and inter-individual variability associated with it	1/day
$KC50$, $\omega KC50$	MMAE concentrations at which the killing rate constant is half of its maximum value, and inter-individual variability associated with it	nM
PL_{Tumor}	Tumor payload concentration responsible for the cytotoxicity	nM
Tau, ωTau	Transduction time between two tumor compartments, and inter-individual variability associated with it	day
ψ	A switch function between exponential and linear growth rates of the tumor	Unitless
$ADC^0_{Extra\_Cellular}$	ADC concentration in the cell culture media at time = 0	nM
$Dose_{PL}$	Dosing amount of payload	Nanomole
DAR^0	Drug antibody ratio for the ADC at time = 0	Unitless
$Dose_{ADC}$	Dosing amount of ADC	Nanomole

In order to validate the aforementioned model, an in vitro experiment from literature, using brentuximab-vedotin as an ADC and two different CD30+ cell lines (L540cy & Karpas299) as experimental systems, was simulated and the results from the simulated experiment were compared with experimental results from Okeley et al. [8]. It was assumed that during the experimental time frame cell killing by the ADC is offset by cell proliferation, and total antigen concentration remains the same. The relevant outputs for comparison were calculated by assuming 5×10^5 cancer cells/ml (L540cy or Karpas299), and a single cell volume of one picoliter. Parameters pertaining to brentuximab-vedotin, for incorporation in the model, were obtained or derived from various publications and are provided in Table 2.

Modeling the PK of MMAE in the plasma and tumor of xenograft mouse (step-2)

A PK model was then developed to characterize the disposition of MMAE at the tissue level. Literature derived plasma and tumor PK of MMAE, after systemic administration of 0.04 mg/kg MMAE in a mouse xenograft model [9], were fitted by the following model equations:

$$\frac{dX1_{PL}}{dt} = -\frac{CL_{PL}}{V1_{PL}} \cdot X1_{PL} - \frac{CLD_{PL}}{V1_{PL}} \cdot X1_{PL} + \frac{CLD_{PL}}{V2_{PL}} \cdot X2_{PL} - \frac{2 \cdot P_{PL} \cdot R_{Cap}}{{R_{Krogh}}^2} \cdot \left(\varepsilon_{PL} \cdot \frac{X1_{PL}}{V1_{PL}} - PL^{Tumor}_{Extra\_Cellular}\right) \cdot TV - \frac{6 \cdot D_{PL}}{{R_{Tumor}}^2} \cdot \left(\varepsilon_{PL} \cdot \frac{X1_{PL}}{V1_{PL}} - PL^{Tumor}_{Extra\_Cellular}\right) \cdot TV; IC = Dose_{PL} \quad (5)$$

$$\frac{dX2_{PL}}{dt} = \frac{CLD_{PL}}{V1_{PL}} \cdot X1_{PL} - \frac{CLD_{PL}}{V2_{PL}} \cdot X2_{PL}; IC = 0 \quad (6)$$

$$\frac{dPL^{Tumor}_{Extra\_Cellular}}{dt} = \frac{2 \cdot P_{PL} \cdot R_{Cap}}{{R_{Krogh}}^2} \cdot \left(\varepsilon_{PL} \cdot \frac{X1_{PL}}{V1_{PL}} - PL^{Tumor}_{Extra\_Cellular}\right) + \frac{6 \cdot D_{PL}}{{R_{Tumor}}^2} \cdot \left(\varepsilon_{PL} \cdot \frac{X1_{PL}}{V1_{PL}} - PL^{Tumor}_{Extra\_Cellular}\right) - k_{int_{PL}} \cdot PL^{Tumor}_{Extra\_Cellular} + k_{out\,PL} \cdot PL^{Tumor}_{Intra\_Cellular}; IC = 0 \quad (7)$$

$$\frac{dPL^{Tumor}_{Intra\_Cellular}}{dt} = k_{int_{PL}} \cdot PL^{Tumor}_{Extra\_Cellular} - k_{out_{PL}} \cdot PL^{Tumor}_{Intra\_Cellular} - k_{on\,Tubulin}^{PL} \cdot PL^{Tumor}_{Intra\_Cellular} \cdot \left(Tubulin_{Total} - PL^{Bound}_{Tubulin}\right) + k_{off\,Tubulin}^{PL} \cdot PL^{Bound}_{Tubulin}; IC = 0 \quad (8)$$

$$\frac{dPL^{Bound}_{Tubulin}}{dt} = k_{on\,Tubulin}^{PL} \cdot PL^{Tumor}_{Intra\_Cellular} \cdot \left(Tubulin_{Total} - PL^{Bound}_{Tubulin}\right) - k_{off\,Tubulin}^{PL} \cdot PL^{Bound}_{Tubulin}; IC = 0 \quad (9)$$

Above, the PK of MMAE in the central and peripheral (except tumor) compartment is described by a simple two compartment model (Eqs. 5 and 6). And, the tumor PK of MMAE is described by a more sophisticated tumor disposition model (Eq. 7), which is an adapted version of a published, clinically translatable tumor disposition model [10–12]. Rather than estimating the tumor distribution parameters for MMAE, the model uses established drug molecular weight and tumor size dependent parameters to drive MMAE from plasma to the tumor extracellular space and vice versa. The model also accounts for entry and exit of payload in the cancer cell, as well as binding of payload to a target in the cell, in a mechanistic manner (Eqs. 8 and 9). Please refer to Table 2 for the parameter values used in the model.

Modeling the PK of brentuximab-vedotin in mouse plasma (step-3)

Plasma PK of brentuximab-vedotin after systemic administration in mouse was characterized by fitting the plasma concentration versus time profiles of brentuximab-vedotin, obtained from two different publications [5, 13], with a two compartment model with linear elimination from the central compartment. In addition, stability of the vc linker in mouse plasma was characterized by fitting the literature derived average DAR versus time profile of brentuximab-vedotin [5] to the following exponential decline equation:

$$\frac{dDAR}{dt} = -k_{dis} \cdot DAR; IC = DAR^0 \quad (10)$$

where k_{dis} is the first order dissociation rate of MMAE from cAC10. Of note, multiple payloads are conjugated on antibody at different locations, and depending on the site of conjugation a payload may have different in vivo stability/residence time on the antibody. Thus, average DAR profile changes with time, and in order to accurately determined umber of payload conjugated to antibody at a given point of time, it is important to well characterize the average DAR versus the time profile for an ADC.

Predicting tumor payload concentrations (step-4)

As the payload concentration in the tumor is the driving force for the efficacy of an ADC, and represents the concentration of active ingredient at the site of action, it is of paramount importance for a PK/PD model to accurately

Table 2 Literature derived or estimated parameter values used in the PK/PD model

Parameter	Value	Unit	Source
Step-1			
Ag_{Total}	0.49 (L540cy), 0.24 (Karpas299)	nM	Calculated from [8]
$k_{on}{}^{ADC}_{Antigen}$	6.22	1/nM/day	Assumed from [36]
$k_{off}{}^{ADC}_{Antigen}$	12.5	1/day	Based on Kd of 2 nM
$k_{int_{Ag}}$	0.61	1/day	Derived from [37]
DAR	4.4	Unitless	From [8]
$k_{out_{PL}}$	1.1 (L540cy), 0.68 (Karpas299)	1/day	Derived from [8]
Step-2			
CL_{PL}	18.4	L/day/Kg	Estimated
$V1_{PL}$	0.136	L/Kg	Estimated
CLD_{PL}	1.84	L/day/Kg	Estimated
$V2_{PL}$	0.523	L/Kg	Estimated
P_{PL}	2.1E + 04	μm/day	http://tumormodel.org
R_{Cap}	8	μm	From [10]
R_{Krogh}	75	μm	From [10]
ε_{PL}	0.44	Unitless	http://tumormodel.org
D_{PL}	0.25	cm^2/day	http://tumormodel.org
R_{Tumor}	Dynamic	cm	Derived from tumor volume
$k_{int_{PL}}$	9.66	1/day	Estimated
$k_{out_{PL}}$	1.1 (L540cy), 0.68 (Karpas299)	1/day	Derived from [8]
$k_{on}{}^{PL}_{Tubulin}$	0.44	1/nM/day	Based on Kd of 30 nM
$k_{off}{}^{PL}_{Tubulin}$	13.1	1/day	Assumed
$Tubulin_{Total}$	65	nM	Estimated
Step-3			
CL_{ADC}	0.006	L/day/Kg	Estimated
$V1_{ADC}$	0.046	L/Kg	Estimated
CLD_{ADC}	0.13	L/day/Kg	Estimated
$V2_{ADC}$	0.06	L/Kg	Estimated
k_{dis}	0.12	1/day	Derived from [5]
Step-4			
P_{ADC}	334	μm/day	http://tumormodel.org
D_{ADC}	0.022	cm^2/day	http://tumormodel.org
ε_{ADC}	0.24	Unitless	http://tumormodel.org
Ag_{Total}	976 (L540cy), 483 (Karpas299)	nM	Calculated
Step-5			
$k_{g_{Exponenial}}$	0.245 (L540cy), 0.278 (Karpas299)	1/day	Estimated
$k_{g_{Linear}}$	43.3 (L540cy), 87.3 (Karpas299)	mm^3/day	Estimated
V_{Max}	5000	mm^3	Estimated
ψ	20	Unitless	Fixed based on [17]
$k_{kill_{Max}}$	0.761 (L540cy), 0.753 (Karpas299)	1/day	Estimated
$KC50$	254 (L540cy), 172 (Karpas299)	nM	Estimated
Tau	0.128 (L540cy), 0.0114 (Karpas299)	day	Estimated
$\omega k_{g_{Exponenial}}$	39.9 (L540cy), 27.3 (Karpas299)	%	Estimated
$\omega k_{g_{Linear}}$	64.9 (L540cy), 65.2 (Karpas299)	%	Estimated
$\omega k_{kill_{Max}}$	20.9 (L540cy), 28.5 (Karpas299)	%	Estimated
$\omega KC50$	25.4 (L540cy), 44.1 (Karpas299)	%	Estimated
ωTau	164 (L540cy), 23.9 (Karpas299)	%	Estimated

Table 2 continued

Parameter	Value	Unit	Source
Step-6			
CL_{ADC}	0.025	L/day/Kg	Estimated
$V1_{ADC}$	0.054	L/Kg	Estimated
CLD_{ADC}	0.036	L/day/Kg	Estimated
$V2_{ADC}$	0.1	L/Kg	Estimated
k_{dis}	0.072	1/day	Derived from [5]
CL_{PL}	0.93	L/day/Kg	Estimated
$V1_{PL}$	1.26	L/Kg	Estimated
CLD_{PL}	3.03	L/day/Kg	Estimated
$V2_{PL}$	0.799	L/Kg	Estimated
Step-7			
Ag_{Total}	166	nM	Calculated from [21]
$k_{g_{Exponenial}}$	0.035	1/day	Derived from [22]
$k_{g_{Linear}}$	220	mm^3/day	Derived from [22]
V_{Max}	5.24E+05	mm^3	Assumed
$V1_{Initial}$	4.19E+03	mm^3	Based on [20]

predict this concentration. To achieve that, a two step process was undertaken where a novel, clinically translatable, tumor disposition model for ADC was developed, which was subsequently evaluated against the published literature data for brentuximab-vedotin. Figure 1 displays a diagram of the integrated multiscale PK/PD model for the ADC. In the model, after systemic administration of brentuximab-vedotin in the central compartment it is either allowed to distribute to the peripheral compartment using parameters obtained in step-3 (modeling the PK of brentuximab-vedotin in mouse plasma), or distribute to the tumor extracellular compartment using the parameters calculated based on the drug molecular weight and tumor size [10–12]. The free payload, either generated in the systemic circulation via nonspecific shedding from ADC or via metabolism of ADC, and generated in the tumor, was characterized using the plasma and tumor specific PK model developed for MMAE in step-2 (modeling the PK of MMAE in the plasma and tumor of xenograft mouse). Once in the tumor extracellular environment, cellular disposition of brentuximab-vedotin and MMAE is characterized using the parameters and model developed based on the in vitro system described in step-1 (modeling the PK of brentuximab-vedotin and MMAE at cellular level). In order to validate the results from this ADC tumor disposition model, MMAE concentrations in tumor, free MMAE concentrations in plasma, and conjugated MMAE concentrations in plasma were simulated in L540cy xenograft bearing mouse after an intravenous 2 mg/kg dose of brentuximab-vedotin. The predicted results were compared with experimental data from the literature [9, 14]. Equations for the integrated ADC tumor disposition model are provided below:

$$\begin{aligned}\frac{dX1_{ADC}}{dt} &= -\frac{CL_{ADC}}{V1_{ADC}}\cdot X1_{ADC} - \frac{CLD_{ADC}}{V1_{ADC}}\cdot X1_{ADC} \\ &\quad + \frac{CLD_{ADC}}{V2_{ADC}}\cdot X2_{ADC} - \frac{2\cdot P_{ADC}\cdot R_{Cap}}{{R_{Krogh}}^2} \\ &\quad \cdot\left(\varepsilon_{ADC}\cdot\frac{X1_{ADC}}{V1_{ADC}} - ADC^{Free}_{Tumor\_ExtraCellular}\right)\cdot TV \\ &\quad - \frac{6\cdot D_{ADC}}{{R_{Tumor}}^2} \\ &\quad \cdot\left(\varepsilon_{ADC}\cdot\frac{X1_{ADC}}{V1_{ADC}} - ADC^{Free}_{Tumor\_ExtraCellular}\right) \\ &\quad \cdot TV;\ IC \\ &\quad = Dose_{ADC} \end{aligned} \tag{11}$$

$$\frac{dX2_{ADC}}{dt} = \frac{CLD_{ADC}}{V1_{ADC}}\cdot X1_{ADC} - \frac{CLD_{ADC}}{V2_{ADC}}\cdot X2_{ADC}; IC = 0 \tag{12}$$

$$\begin{aligned}\frac{dADC^{Free}_{Tumor\_ExtraCellular}}{dt} &= \frac{2\cdot P_{ADC}\cdot R_{Cap}}{{R_{Krogh}}^2} \\ &\cdot\left(\varepsilon_{ADC}\cdot\frac{X1_{ADC}}{V1_{ADC}} - ADC^{Free}_{Tumor\_ExtraCellular}\right) + \frac{6\cdot D_{ADC}}{{R_{Tumor}}^2} \\ &\cdot\left(\varepsilon_{ADC}\cdot\frac{X1_{ADC}}{V1_{ADC}} - ADC^{Free}_{Tumor\_ExtraCellular}\right) - k_{on}{}^{ADC}_{Antigen} \\ &\cdot ADC^{Free}_{Tumor\_ExtraCellular}\cdot\left(Ag_{Total} - ADC^{Bound}_{Tumor\_ExtraCellular}\right) \\ &+ k_{off}{}^{ADC}_{Antigen}\cdot ADC^{Bound}_{Tumor\_ExtraCellular}; IC = 0 \end{aligned} \tag{13}$$

$$\frac{dADC^{Bound}_{Tumor\_ExtraCellular}}{dt} = k^{ADC}_{on\,Antigen} \cdot ADC^{Free}_{Tumor\_ExtraCellular} \cdot \left(Ag_{Total} - ADC^{Bound}_{Tumor\_ExtraCellular}\right) - k^{ADC}_{off\,Antigen} \cdot ADC^{Bound}_{Tumor\_ExtraCellular} - k_{int_{Ag}} \cdot ADC^{Bound}_{Tumor\_ExtraCellular}; IC = 0 \quad (14)$$

$$\frac{dPL^{Tumor}_{Intra\_Cellular}}{dt} = k_{int_{Ag}} \cdot ADC^{Bound}_{Tumor\_ExtraCellular} \cdot DAR + k_{int_{PL}} \cdot PL^{Tumor}_{Extra\_Cellular} - k_{out_{PL}} \cdot PL^{Tumor}_{Intra\_Cellular} - k^{PL}_{on\,Tubulin} \cdot PL^{Tumor}_{Intra\_Cellular} \cdot \left(Tubulin_{Total} - PL^{Bound}_{Tubulin}\right) + k^{PL}_{off\,Tubulin} \cdot PL^{Bound}_{Tubulin}; IC = 0 \quad (15)$$

$$\frac{dPL^{Bound}_{Tubulin}}{dt} = k^{PL}_{on\,Tubulin} \cdot PL^{Tumor}_{Intra\_Cellular} \cdot \left(Tubulin_{Total} - PL^{Bound}_{Tubulin}\right) - k^{PL}_{off\,Tubulin} \cdot PL^{Bound}_{Tubulin};\ IC = 0 \quad (16)$$

$$\frac{dPL^{Tumor}_{Extra\_Cellular}}{dt} = \frac{2 \cdot P_{PL} \cdot R_{Cap}}{{R_{Krogh}}^2} \cdot \left(\varepsilon_{PL} \cdot C1_{PL} - PL^{Tumor}_{Extra\_Cellular}\right) + \frac{6 \cdot D_{PL}}{{R_{Tumor}}^2} \cdot \left(\varepsilon_{PL} \cdot C1_{PL} - PL^{Tumor}_{Extra\_Cellular}\right) - k_{int_{PL}} \cdot PL^{Tumor}_{Extra\_Cellular} + k_{out_{PL}} \cdot PL^{Tumor}_{Intra\_Cellular} + DAR \cdot k_{dis} \cdot \left(ADC^{Free}_{Tumor\_ExtraCellular} + ADC^{Bound}_{Tumor\_ExtraCellular}\right); IC = 0 \quad (17)$$

$$\frac{dC1_{PL}}{dt} = -\frac{CL_{PL}}{V1_{PL}} \cdot C1_{PL} - \frac{CLD_{PL}}{V1_{PL}} \cdot C1_{PL} + \frac{CLD_{PL}}{V2_{PL}} \cdot C2_{PL} - \frac{2 \cdot P_{PL} \cdot R_{Cap}}{{R_{Krogh}}^2} \cdot \left(\varepsilon_{PL} \cdot C1_{PL} - PL^{Tumor}_{Extra\_Cellular}\right) \cdot TV - \frac{6 \cdot D_{PL}}{{R_{Tumor}}^2} \cdot \left(\varepsilon_{PL} \cdot C1_{PL} - PL^{Tumor}_{Extra\_Cellular}\right) \cdot TV + \frac{X1_{ADC} \cdot DAR \cdot Kdis}{V1_{PL}} + \frac{CL_{ADC} \cdot DAR \cdot \frac{X1_{ADC}}{V1_{ADC}}}{V1_{PL}};\ IC = 0 \quad (18)$$

$$\frac{dC2_{PL}}{dt} = \frac{CLD_{PL}}{V1_{PL}} \cdot C1_{PL} - \frac{CLD_{PL}}{V2_{PL}} \cdot C2_{PL};\ IC = 0 \quad (19)$$

Equations 11 and 12 describe the plasma PK of ADC, and Eqs. 13 and 14 describe the tumor PK of ADC. Equations 15–17 describe the tumor PK of payload, and Eqs. 18 and 19 describe the plasma PK of payload. Since the released payload for brentuximab-vedotin (i.e. MMAE) demonstrates bystander effects, total tumor payload concentration (calculated as the sum of $PL^{Tumor}_{Intra\_Cellular}$, $PL^{Bound}_{Tubulin}$ and $PL^{Tumor}_{Extra\_Cellular}$) was used to drive the efficacy instead of just using the intercellular payload concentration.

Modeling the preclinical efficacy of brentuximab-vedotin (step-5)

In order to quantify the PD parameters for brentuximab-vedotin, tumor growth inhibition (TGI) data from two different xenograft (L540cy and Karpas299) bearing mouse models, treated with various doses of brentuximab-vedotin, were obtained from the literature [9, 13, 15, 16]. The TGI data were subsequently modeled using the population PK/PD model, where the tumor PK of brentuximab-vedotin and MMAE were described using the model built in step-4 (predicting tumor payload concentrations), and the PD was modeled using an adapted cell distribution model [7, 17, 18]. Equations for the PD model are provided below:

$$\frac{dV1}{dt} = \frac{k_{g_{Exponenial}} \cdot \left(1 - \frac{TV}{V_{Max}}\right) \cdot V1}{\left(1 + \left(\frac{k_{g_{Exponenial}}}{k_{g_{Linear}}} \cdot TV\right)^{\psi}\right)^{1/\psi}} - \frac{k_{kill_{Max}} \cdot PL_{Tumor}}{KC50 + PL_{Tumor}} \cdot V1;\ IC = V1_{Initial} \quad (20)$$

$$\frac{dV2}{dt} = \frac{k_{kill_{Max}} \cdot PL_{Tumor}}{KC50 + PL_{Tumor}} \cdot V1 - \frac{V2}{Tau};\ IC = 0 \quad (21)$$

$$\frac{dV3}{dt} = \frac{(V2 - V3)}{Tau};\ IC = 0 \quad (22)$$

$$\frac{dV4}{dt} = \frac{(V3 - V4)}{Tau};\ IC = 0 \quad (23)$$

$$TV = V1 + V2 + V3 + V4 \quad (24)$$

Equation 20 describe the growth and payload induced killing phenomenon for the tumor. Equations 21–23 describes the non-growing fraction of tumor that is destined for death. And, Eq. 24 describes the total tumor volume. The tumor is allowed to grow initially in an exponential manner with switches to a linear growth rate as the size of the tumor increases. Once the tumor cells are exposed to the payload, they are shuttled to a non-growing transduction compartment, from where these cells are destined to die with a rate determined by the transduction parameter *Tau*. The killing rate of the tumor is described as a nonlinear function of total released payload concentration inside the tumor. All the TGI

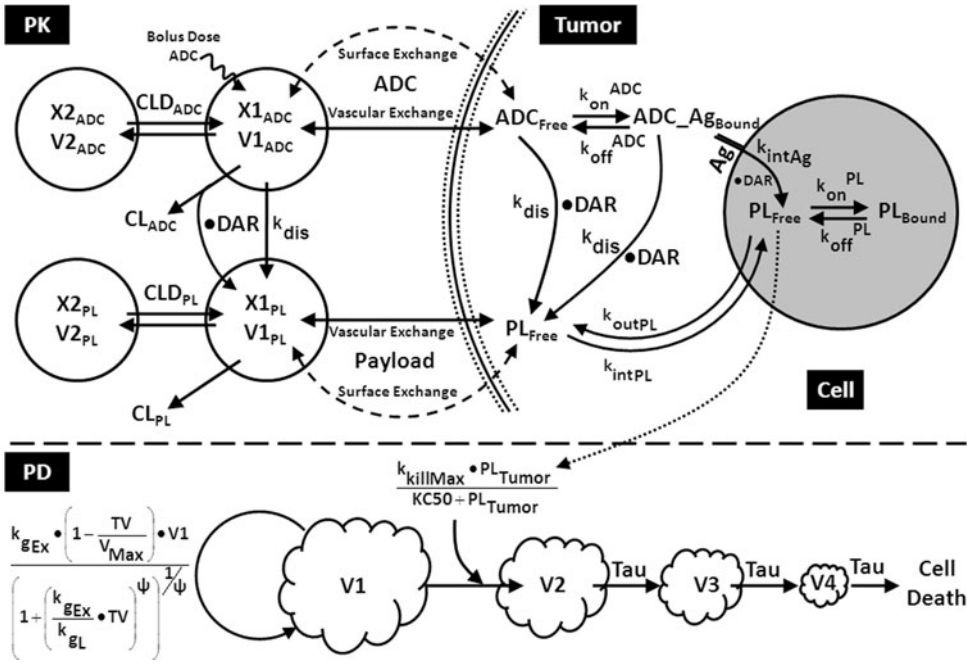

Fig. 1 The PK/PD Model. A schematic diagram of the proposed PK/PD model for ADC is shown. *PK*: After administration of ADC into the systemic circulation, the ADC can distribute to the peripheral compartment, be eliminated, or distribute to the tumor compartment. Once inside the tumor extracellular matrix, the ADC is either allowed to interact with the cell surface antigen or allowed to diffuse back to the systemic circulation. The surface bound ADC is allowed to internalize into the cancer cell, where it is assumed to be degraded. Each molecule of degraded ADC is assumed to generate certain molecules of payload in the cell, equivalent to the DAR of the ADC at the given time. The free payload in the cell is allowed to bind to the target or allowed to exit to the extracellular matrix. In the extracellular space the free payload can also be generated from its dissociation to free or bound ADC. Free payload from tumor extracellular matrix is allowed to exchange between the plasma and tumor in a similar manner as ADC, or allowed to go back in the tumor cells. Once inside the systemic circulation, the payload is allowed to distribute to the peripheral compartment, be eliminated, or distribute back to the tumor compartment. *PD*: Please refer to "Modeling the preclinical efficacy of brentuximab-vedotin (step-5)" sub-section in "Model development" section for more detail about the PD model

data for brentuximab-vedotin from a given xenograft model were fitted simultaneously to Eqs. 20–24 to estimate the PD parameter and inter-individual variability associated with them.

Modeling the PK of brentuximab-vedotin and MMAE in the plasma of cancer patients (step-6)

Clinical PK of brentuximab-vedotin and MMAE from two different clinical trials, employing two different dosing regimens, was obtained from the literature [19, 20]. Both trials had PK data from a multiple dosing study for several doses. A simple two compartmental model with linear elimination from the central compartment was used to characterize the PK of brentuximab-vedotin and MMAE. Any nonspecifically shed MMAE from brentuximab-vedotin, or MMAE generated from the eliminated brentuximab-vedotin, was introduced back into the central compartment of the MMAE model, as shown in Eq. 18. The dissociation rate (k_{dis}) of MMAE from brentuximab-vedotin in human plasma was assumed to be the same as in monkey, which was obtained from literature [5].

Preclinical to clinical translation of the ADC PK/PD model (step-7)

The integrated PK/PD model, described in steps 4 and 5, was used to perform clinical trial simulations for brentuximab-vedotin. However, to enable preclinical to clinical translation the following changes were made to the model parameters: (a) The number of CD30 receptors on cancer cells were changed to the value obtained from a cancer patient [21], (b) The growth rate of the tumor was set to match clinically observed values [22], (c) clinical PK parameters for brentuximab-vedotin and MMAE were adopted from step-6 (modeling the PK of brentuximab-vedotin and MMAE in the plasma of cancer patients) estimates, and (d) the initial tumor burden and maximum possible tumor burden were set to clinically observed/plausible values [20]. The rest of the parameter values, including the inter-individual variability in PD parameters, were kept the same as in the preclinical case. Please refer to Table 2 for the parameter values.

In order to evaluate the predictive performance of the translated parameters and the ADC PK/PD model, two

different clinical trials for brentuximab-vedotin were simulated using the parametric simulation method [23]. In each trial 1,000 patients were simulated for each dose. One trial explored a once every 3 week dosing regimen for seven cycles (0.1–2.7 mg/kg) [19], and the other explored a once a week dosing regimen for 3 week followed by a 1 week gap for two cycles (0.4–1.4 mg/kg) [20, 24]. From each simulated clinical trial, the PFS and response rates were calculated and compared with the results from actual clinical trials [19, 20, 24], to evaluate the predictability and preclinical to clinical translation ability of the proposed mechanistic PK/PD model for ADCs. The PFS rates were calculated periodically using the following schedule: every week for the first 42 days, then onwards every 2 weeks up to 210 days, then every month up to 360 days, and every 2 months for the rest of the period. A spherical shape was assumed for the tumor, and the diameter of the tumor was calculated from the tumor volume, using the volumetric equation for the spherical shape. The criteria to categorize response rates for progressive disease, stable disease (SD), partial regression (PR), and complete regression (CR) were: more than 20 % increase in tumor diameter, less than 30 % reduction in tumor diameter, more than 30 % decrease in tumor diameter but still detectable, and below the detection limit of 0.5 cm tumor diameter, according to the *Revised Response Criteria for Malignant Lymphoma* [25].

Data collection and model implementation

All the datasets used for model development and validation were digitized from the literature (using the software 'Grab It! XP'). Models were fitted to the data using the maximum likelihood (ML) estimation method in the ADAPT-5 software (BMSR, CA) [26] with the combined (proportional + additive) variance model. All the simulations were performed using the software Berkeley Madonna (University of California at Berkeley, CA).

Results

Modeling the PK of brentuximab-vedotin and MMAE at cellular level (step-1)

Intracellular and extracellular MMAE concentration versus time profiles were simulated mimicking incubation of 200 ng/ml (1.33 nM) brentuximab-vedotin with 5×10^5 L540cy or Karpas299 cells/ml. Simulated profiles for L540cy or Karpas299 cell lines were compared with the observed results from in vitro experiments conducted by Okeley et al. [8] in Fig. 2a and b, respectively. In general, the model predicted concentration versus time profiles of intracellular and extracellular MMAE, for both cell lines, reasonably well. Consistent with experimental results, the model predicted that intracellular MMAE concentrations would be more than 100 times MMAE concentration in media. Simulated intracellular MMAE concentrations were slightly lower than observed concentration, suggesting a possible binding site for MMAE inside the cell, which was not considered in the in vitro model (Eqs. 1–4). Extracellular MMAE concentrations were under predicted at earlier time points, suggesting a possible contribution of MMAE shed from brentuximab-vedotin, which was not considered in the model due to the assumption of ADC stability in the cell culture media.

Modeling the PK of MMAE in the plasma and tumor of xenograft mouse (step-2)

Figure 3a and b shows model fits to observed data for MMAE concentration versus time profiles in the plasma and tumor of L540cy xenograft mouse, after a bolus dose of 0.04 mg/kg MMAE. The model was able to characterize both the profiles well with reasonable confidence in the parameter estimates, which are shown in Table 2 and Supplementary Table 1. Of note, as hypothesized in the analysis of step-1 (modeling the PK of brentuximab-vedotin and MMAE at cellular level) results, incorporation of intracellular tubulin binding was necessary to characterize tumor MMAE concentrations.

Modeling the PK of brentuximab-vedotin in mouse plasma (step-3)

Brentuximab-vedotin plasma PK in mouse, obtained from two different publications [5, 13], was well characterized with a two compartment model (Fig. 3c). Model estimates are provided in Table 2. Exponential decay also well characterized the average DAR versus time profile for brentuximab-vedotin in mouse, with the dissociation half life of MMAE $\sim$6 days.

Predicting tumor payload concentrations (step-4)

Figure 3d shows simulated MMAE concentrations in tumor, free MMAE concentrations in plasma, and conjugated MMAE concentrations in plasma of L540cy xenograft bearing mouse superimposed over experimental results from literature [9]. As evident in the figure, the model predicted reasonably well all the profiles using a predefined set of parameters, without estimating any parameters, thus providing confidence in the ability of the

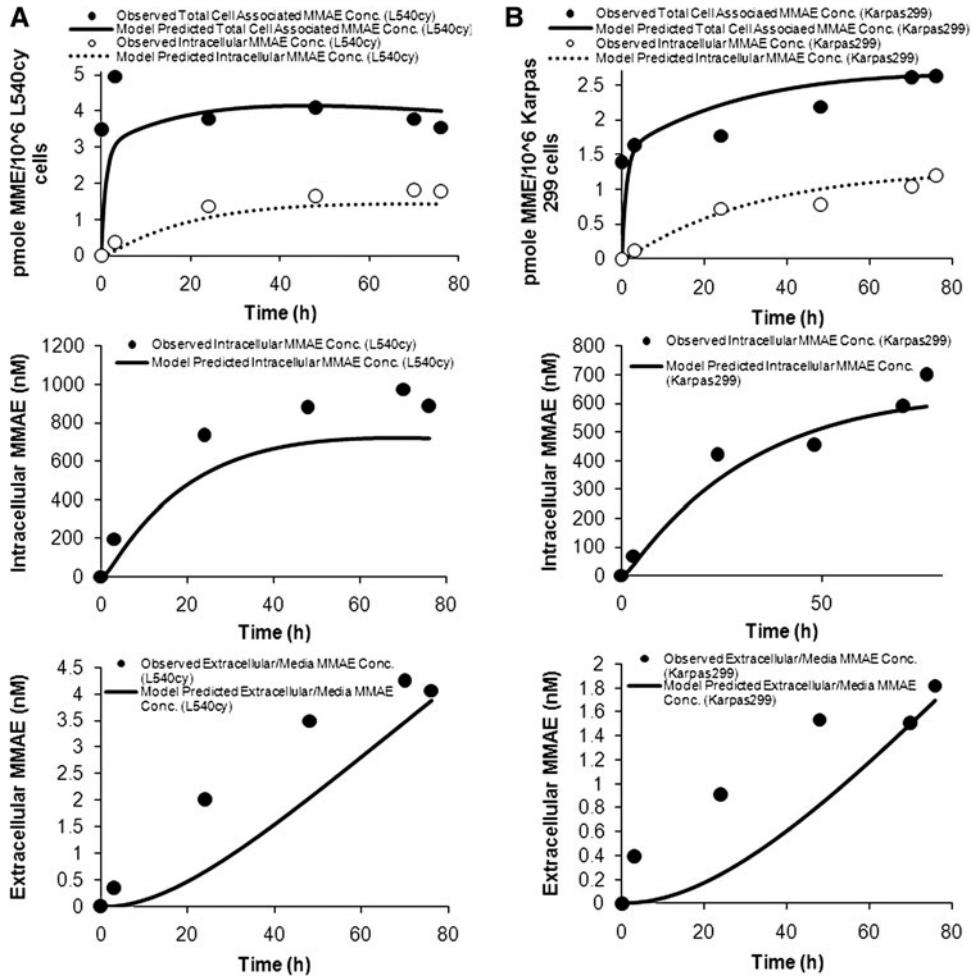

Fig. 2 Cellular level PK of brentuximab-vedotin and MMAE. Extracellular and intracellular concentrations of MMAE were simulated after incubating 200 ng/ml (1.33 nM) of brentuximab-vedotin with 5×10^5 L540cy or Karpas299 cells/ml. The simulated profiles were compared with the observed data from literature, which followed the same experimental protocol. **a** *Upper panel*: *solid line* represents simulated total cell associated MMAE concentrations and *dotted line* represents simulated intracellular MMAE concentrations in L540cy cells, represented as pmoles of MMAE per million cells. *Solid circles* represent total and *open circles* represent intracellular observed concentrations. *Middle panel: solid line* represents simulated and *solid circles* represent observed intracellular MMAE concentrations in L540cy cells (in nM). *Lower panel*: *solid line* represents simulated and *solid circles* represent observed extracellular MMAE concentrations in media containing L540cy cells (in nM). **b** Data description in panel B is similar to panel A, except the cell line being used is Karpas299 instead

novel ADC tumor disposition model to predict payload concentration at the site of action.

Modeling the preclinical efficacy of brentuximab-vedotin (step-5)

Figure 4a, b show the fitting of TGI data, from different doses and dosing regimens, for L540cy and Karpas299 bearing xenografts using the proposed PK/PD model. All the data for a given cell line was fitted simultaneously using a population model, and the parameter estimates are provided in Table 2. The model was able to characterize the data well, providing a set of PD parameters for preclinical to clinical translation of brentuximab-vedotin efficacy.

Modeling the PK of brentuximab-vedotin and MMAE in the plasma of cancer patients (step-6)

The two compartment model was able to characterize the multiple dose clinical PK of brentuximab-vedotin and MMAE reasonably well (Fig. 5). Table 2 provides the estimates for brentuximab-vedotin and MMAE clinical PK, which were utilized for clinical trial simulations.

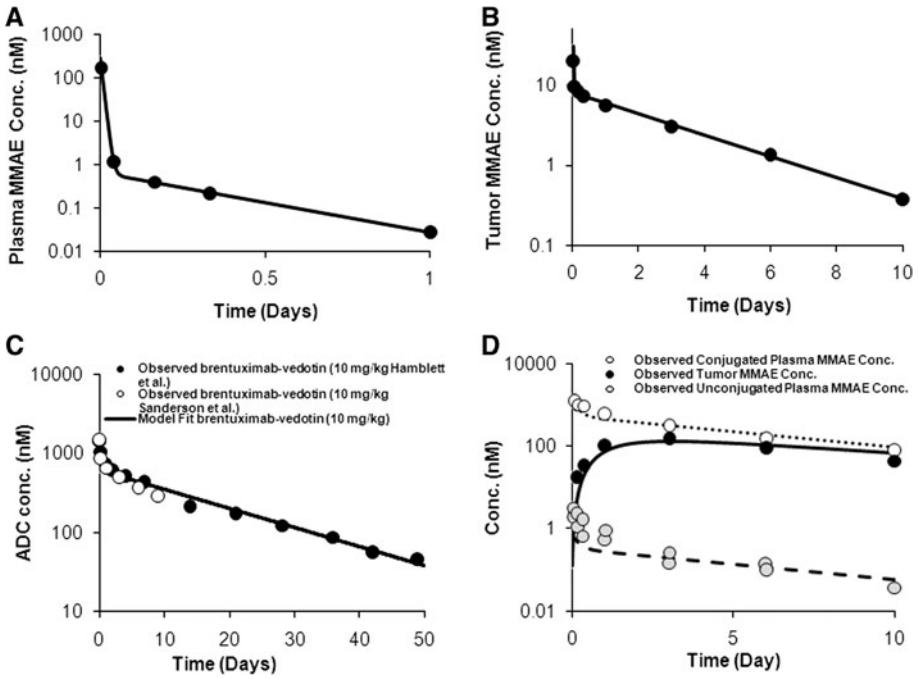

Fig. 3 Plasma and tumor PK of MMAE and brentuximab-vedotin. **a** Observed (*solid circles*) and model fitted (*solid line*) plasma MMAE concentration versus time profile after injecting 0.04 mg/kg MMAE in tumor bearing mouse. **b** Observed (*solid circles*) and model fitted (*solid line*) tumor MMAE concentration versus time profile after injecting 0.04 mg/kg MMAE in tumor bearing mouse. **c** Observed (*solid and open circles* represents data from two different publications) and model fitted (*solid line*) plasma brentuximab-vedotin concentration versus time profile after injecting 10 mg/kg brentuximab-vedotin in mouse. **d** *Solid line* represents model simulated and *solid circles* represent observed tumor MMAE concentrations, *dashed line* represents model simulated and the *gray circles* represent observed free plasma MMAE concentrations, *dotted line* represents model simulated and *open circles* represent observed total plasma MMAE concentrations, in a tumor bearing mouse, which was injected with 2 mg/kg of brentuximab-vedotin

Preclinical to clinical translation of the ADC PK/PD model (step-7)

Considering most of the patients, in both the clinical trials evaluated, were Hodgkin's lymphoma patients, preclinical PD values from Hodgkin-derived L540cy cell line xenografts were used to simulate the clinical trials. The first clinical trial was simulated using the regimen one dose given every 3 weeks (Q3W), for seven dosing cycles at eight dosages, to mimic the treatment in the published clinical trial [19]. Figure 6a compares the simulated and observed PFS for Q3W trial, demonstrating that the simulated results were very close to the PFS rates observed in the actual clinical trial. Figure 6b provides the simulated changes in response rates with the dose for the Q3W regimen. Good agreement was seen between the simulated and the observed [19] 'percentage of patients with CR versus dose' profiles (Fig. 6c).

The second clinical trial was simulated using a per cycle regimen of one dose each week (QW) three times followed by a gap of 1 week, for two cycles and six doses, to mimic the treatment in the published clinical trial [24]. Figure 6d provides the comparison for the simulated PFS versus observed for the QW trial, demonstrating that for this trial as well the results from simulated clinical trial were very close to the survival rates observed in the actual clinical trial. Simulated changes in response rates with dose for the QW regimen are provided in Fig. 6e. Figure 6f provides the comparison of simulated 'percentage of patients with CR versus dose' profile to the observed one [24], demonstrating a reasonable agreement between them except for the middle two doses of 0.8 and 1.0 mg/kg.

Discussion

For small or large molecule anti-cancer drugs, bench to bedside translation of efficacy has been challenging. Despite the use of established in vitro and preclinical experimental systems to create confidence in the translation of the drug, and the use of mathematical models to predict clinical efficacy of the drug by integrating/interpreting these data, success rates for oncology clinical trials are unacceptably low [27, 28]. One of the main reasons for the aforementioned scenario is a poor appreciation of PK/PD [29], and the use of empirical approaches and mathematical

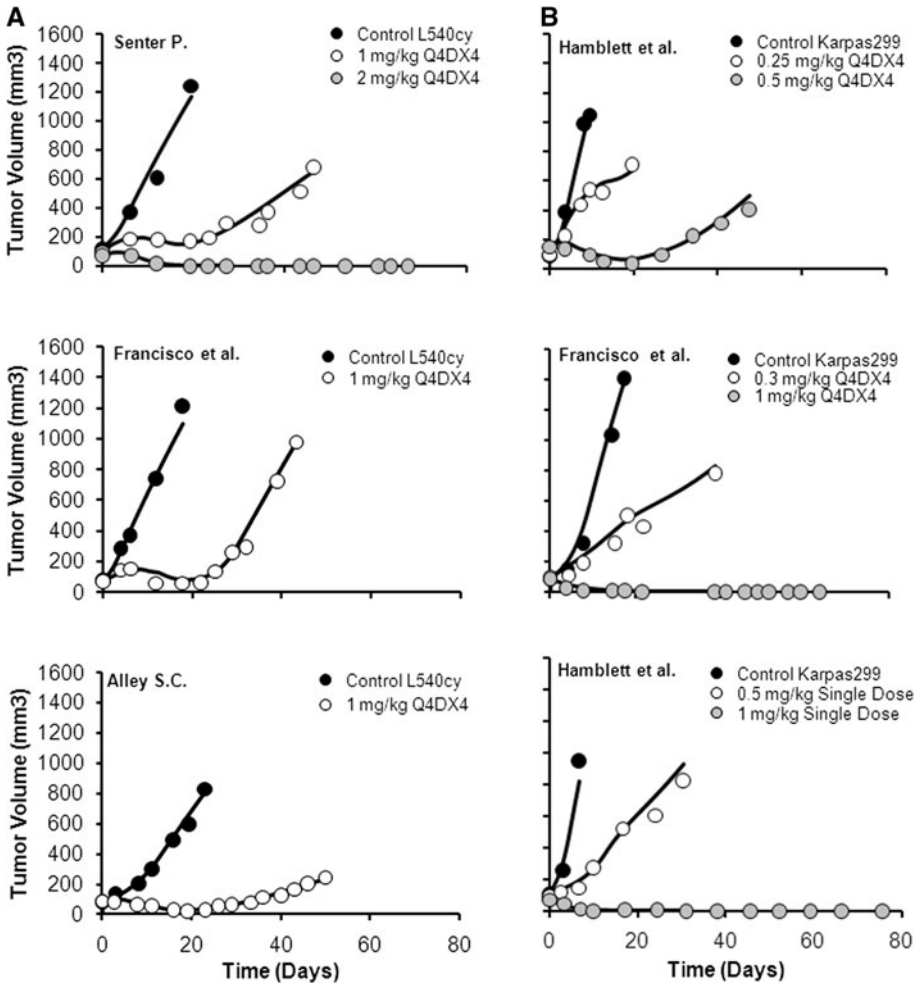

Fig. 4 Characterization of tumor growth inhibition (TGI) data with the PK/PD Model. **a** TGI data obtained from various publications, after injecting diverse doses of brentuximab-vedotin into the L540cy xenograft tumor bearing mouse, were simultaneously characterized using the PK/PD model. The *symbols* represent observed data and the *solid lines* represent model fittings. **b** TGI data obtained from various publications, after injecting diverse doses of brentuximab-vedotin into the Karpas xenograft tumor bearing mouse, were simultaneously characterized using the PK/PD model. The *symbols* represent observed data and the *solid lines* represent model fittings

models with mechanistically unidentifiable parameters (which are mainly suitable just for describing the data and interpolation), to integrate preclinical data and predict/extrapolate the clinical efficacy of drug [30]. This leads to fewer successful bench to bedside translation predictions, and diminished confidence in the importance of in vitro (cell culture) and preclinical (xenograft) experimental systems. Thus, for a novel anti-cancer modality like ADC, which contains both a small and a large molecule, it can be presumed that traditional empirical models may not be ideal to integrate in vitro and preclinical experimental systems with the intent of predicting clinical efficacy.

We describe a step-by-step approach to develop a mechanistically detailed and modality specific platform mathematical model for ADC, which is capable of preclinical to clinical translation. Where part of the model were built and verified at each step to instill quality. In the first step, the fate of the ADC was analyzed after incubating with cancer cells in vitro, which would provide an understanding of the PK of ADC at a cellular level mimicking the extracellular milieu of the tumor. The main goal of the first step was to integrate different biomeasures of ADC brentuximab-vedotin (e.g. internalization rate of brentuximab-vedotin, CD30 receptor number per cell, exit rate of MMAE from the cell, binding affinity of brentuximab-vedotin for CD30) using a simple mathematical model to evaluate how well one can predict the fate of brentuximab-vedotin at the cellular level a priori, using just published values of biomeasures, without estimating any parameters by fitting. Figure 2 demonstrates that it may be possible to predict intracellular and extracellular concentrations of payload using a mathematical model, provided the necessary biomeasure information is available in a quantitative format. It is also important to note that the intracellular concentrations of payload (MMAE) were found to be more than 100 times higher that the concentration of total payload in media, suggesting one should be cautious in correlating cell culture viability data with media payload concentration to assign IC50 values. The media concentration may not accurately reflect the payload concentration inside the cell necessary to induce cytotoxicity, so we recommend that for ADCs, cell culture viability data should be correlated with intracellular payload concentrations.

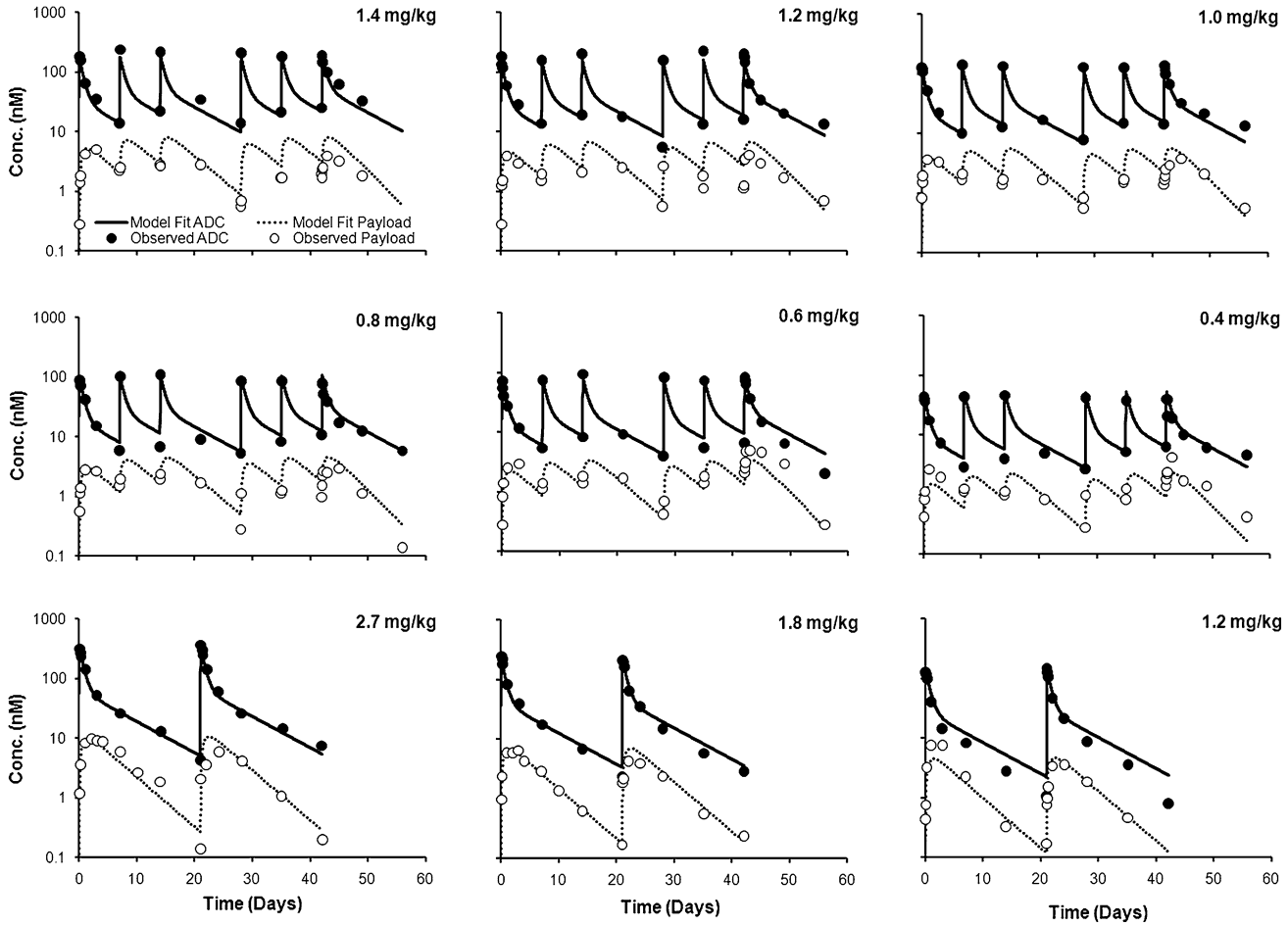

Fig. 5 Characterizing clinical PK of brentuximab-vedotin and MMAE. Plasma PK of brentuximab-vedotin and MMAE, obtained from patients belonging to two different clinical trials with different dosing regimen, were fitted simultaneously to estimate the clinical PK parameters for brentuximab-vedotin and MMAE. The *solid line* represents model fitted brentuximab-vedotin concentrations, and the *dotted line* represents model fitted MMAE concentrations. The *solid circles* represent clinically observed brentuximab-vedotin concentrations, and the *open circles* represent clinically observed MMAE concentrations

In order to estimate the PK parameters for the payload, the second step evaluated plasma and tumor PK of MMAE in tumor bearing mice, after injecting MMAE. As shown in Fig. 3a and b, being a small molecule the payload had a very fast clearance from the plasma; however it lingered in the tumor for a very long time. Considering the PK model accounts for the slower diffusion process of payload between plasma and tumor, the results suggest binding of MMAE in the tumor compartment, leading to a longer tissue half-life. As plasma ADC concentrations are the main driving force for the concentrations of ADC in tumor, the third step estimated parameters for the plasma PK of brentuximab-vedotin, which was well characterized by a simple two compartment model. The third step also evaluated stability of the payload on the ADC by estimating how fast the payload is dissociating from the ADC, providing an accurate determination of the DAR for ADCs that would internalize into cancer cells.

One of the main hurdles for developing a clinically translatable tumor disposition model is the lack of mechanistic and reliable drug exchange parameters between plasma and tumor compartments, which are mainly estimated based on preclinical data. To overcome this problem we have adapted a novel tumor disposition model from the field of biomedical engineering [10–12], which is capable of predicting tumor concentrations of various size molecules in large vascularized tumors, as well as avascular micrometastases. In order to evaluate the tumor disposition model developed specifically for ADCs (Fig. 1), in step-4, all the available parameter values for brentuximab-vedotin and MMAE (from steps 1–3) were incorporated into the model and its predictive ability was assessed. As shown in Fig. 3d the model was able to predict the tumor MMAE concentrations and also the plasma concentrations of MMAE remarkably well, using parameters from sub-models developed in previous steps. Subsequently, in step-5,

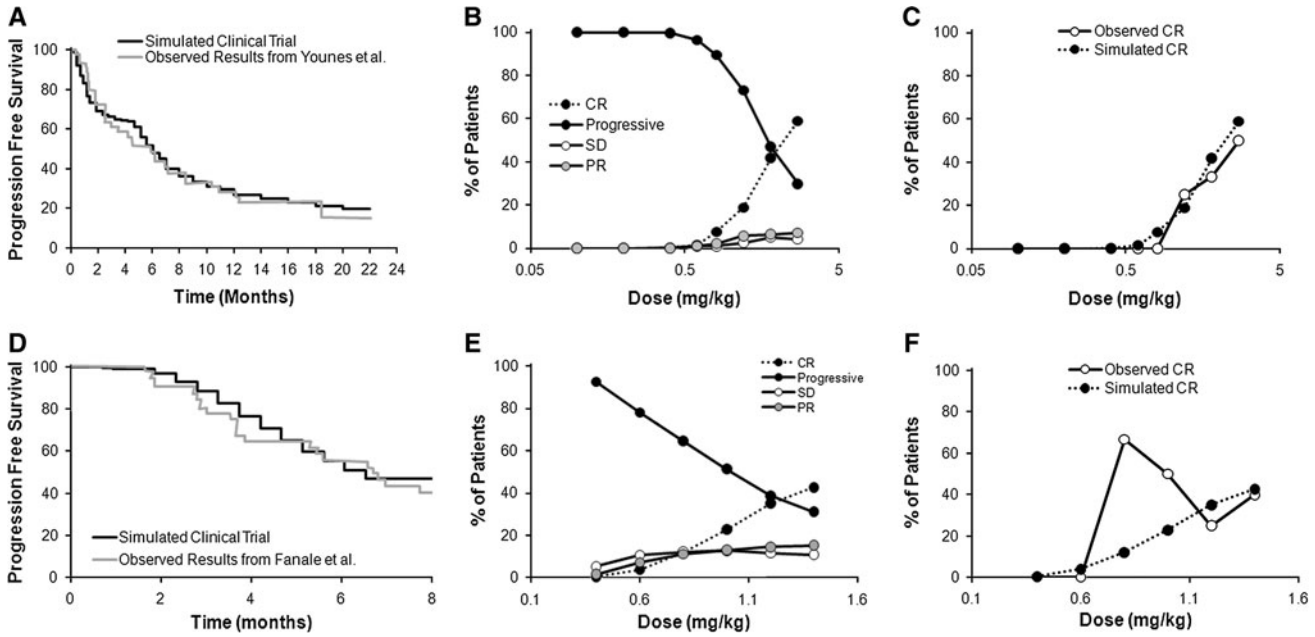

Fig. 6 Comparison of clinical trial simulations with the results from clinical trials. **a** The *solid black line* represents progression free survival rates simulated after dosing brentuximab-vedotin once every 3 weeks (Q3W) for seven cycles (0.1–2.7 mg/kg) in Hodgkin's Lymphoma patients, and the *grey line* represents progression free survival rates observed in patients who were administered brentuximab-vedotin with the same doses and dosing regimen. **b** Simulated percentage of patients receiving certain response at the end of the study (i.e. progressive, stable disease (SD), partial regression (PR), or complete regression (CR)) vs. dose profiles for the Q3W clinical trial simulations. **c** Comparison of the simulated (*solid circles*) and observed (*open circles*) %CR versus dose profiles generated for the Q3W trial. **d** The *solid black line* represents progression free survival rates simulated after dosing brentuximab-vedotin once a week for 3 weeks followed by a gap for 1 week (QW) for two cycles (0.4–1.4 mg/kg) in Hodgkin's Lymphoma patients, and the *grey line* represents progression free survival rates observed in patients who were administered brentuximab-vedotin with the same doses and dosing regimen. **e** Simulated percentage of patients receiving certain response at the end of the study (i.e. progressive, SD, PR, or CR) versus dose profiles for the QW clinical trial simulations. **f** Comparison of the simulated (*solid circles*) and observed (*open circles*) %CR versus dose profiles generated for the QW trial

the validated tumor disposition model was combined with a semi-mechanistic PD model, in which tumor payload concentrations were used to drive efficacy. A unique feature of the proposed PK/PD model is the dynamic interaction incorporated between tumor distribution parameters and tumor size, where changes in tumor volume are directly able to influence the concentration of payload in tumor, which in turn is responsible for the size of the tumor. As shown in Fig. 4, the PK/PD model was able to characterize brentuximab-vedotin preclinical TGI data from various publications reasonably well, providing estimates of the efficacy parameters and the inter-individual variability associated with them.

The next step in the process was to translate/humanize the preclinical PK/PD parameters, while keeping the model structure the same, to predict clinical efficacy of brentuximab-vedotin. To accomplish that, in step-6, the clinical PK parameters for brentuximab-vedotin and MMAE were estimated. The dissociation rate of payload from ADC in human was assumed to be similar to the monkey [5]. Since the parameters for tumor disposition are clinically translatable, they were kept the same. For translating, PD parameters were divided into system specific (e.g. growth rates) and drug specific (e.g. IC50) parameters, and only system specific parameters were changed to match Hodgkin's lymphoma. The initial tumor diameter was chosen to be 2 cm and the highest possible tumor diameter was chosen to be 10 cm. Based on literature [22], the growth rates were adjusted so that the exponential growth doubling time was 20 days and the linear growth doubling time ranged from 20 to 140 days. In step-7, two different clinical trials employing different dosing regimens were simulated using a parametric simulation method, results from which are provided in Fig. 6. It was very interesting to observe that, for both the trials, predicted PFS were superimposable on the observed values. In addition, the predicted CR versus Dose profiles were also comparable for both trials. Of note, the observed percentage of patients with CR for the 0.8 and 1.0 mg/kg doses from QW study were higher than the simulated values (Fig. 6F). This could be because only those two doses had highest number of (50 %) patients with ALCL [20], which is much more responsive than HL after brentuximab-vedotin treatment. Thus, the simulations performed based on parameters for HL, predicted lower percentage of patients with CR

compared to the observation. As such, aforementioned results suggest that a mechanistic mathematical model may be able to predict clinical efficacy of ADCs, provided a correct set of parameters and appropriate translation strategy are chosen.

Of note, the seven step procedure mentioned here provides a framework for using the platform model, which should be followed while keeping in mind the cancer being targeted and the combination of antibody-linker-payload being developed. For example, since MMAE demonstrates bystander effects [8], the entire tumor concentrations were used to drive efficacy. However, in the absence of bystander effects, one might want to correlate the intracellular payload concentration to efficacy. If one has a payload that is non-permeable, characterization of its PK (step-2) may not be necessary for efficacy. In the case of brentuximab-vedotin clinical translation, the value of the killing rate constant ($k_{kill_{Max}}$) was kept the same as estimated in preclinical experiments. However, if one has a means to determine the direction and extent of change in $k_{kill_{Max}}$ needed for a proper clinical translation of efficacy, based on the clinical tumor growth parameters, it should be incorporated.

Apart from a quantitative tool for preclinical to clinical translation of ADC efficacy, the PK/PD model presented here has many other implications. The model can be used to characterize in a mechanistic way the time dependent development of clinical resistance to ADCs due to over expression of efflux transporters by changing the drug efflux rate (k_{out_PL}) over the period of time. Of note, based on the sensitivity analysis of the model (unpublished data) authors hypothesize k_{out_PL} as one of the very important parameters; we believe whose importance is probably often undervalued by the ADC community. Assuming similar internalization rates for an ADC, different payload exit rates from the cell can produce significantly different intracellular payload concentrations, leading to huge differences in the efficacy one may see for a given ADC. The model is also very valuable in determining the number of receptors per cell needed to achieve a certain intracellular payload concentrations, paving a way for precision/personalized medicine scientists to stratify patients based on certain threshold receptor numbers. One can develop a similar model to correlate toxicity of the ADCs with ADC or payload concentrations, providing a more stringent tool for the prediction of overall benefit to risk ratio of ADCs in the clinic.

The presented model is more mechanistic and tailored towards ADCs compared to other published TGI PK/PD models [7, 17, 31, 32]. It is a first of its kind model that characterizes the disposition of antibody and payload separately, and considers changes in DAR over the period of time by accounting for loss/shedding of payload routinely observed in the experiential setting. The model is also designed to gain an integrated understanding of the fundamental PK/PD principles of exposure at the site of action, target binding, and expression of functional pharmacological activity; termed together as the 'three Pillars of survival' [33]. Where the Pillar-1 deals with the fundamental principle that the drug exposure at the target site of action is necessary to elicit a pharmacological effect over a desired time period. Pillar-2 deals with the fundamental principle that target occupancy is a prerequisite for expression of pharmacology and target modulation. And, Pillar-3 deals with the fundamental principle that functional modulation of the target is a prerequisite for expression of pharmacological activity to test the mechanism of action [33]. Rather than using plasma ADC concentration to drive the efficacy, the model attempts to characterize the drug exposure at the target site of action (i.e. Pillar-1 for drug development) [33], and uses tumor payload concentration to drive the efficacy. However, there are still some empirical components in the model. And, to develop a truly mechanistic model to address the Pillar-2 (i.e. binding to the pharmacological target) and Pillar-3 (i.e. expression of pharmacology) of drug development [33], moving forward we intend to elaborate on the presented mechanistic model. We plan to expand the model to be able to incorporate different cell population in the tumor, by incorporating the details similar to the one presented in the cellular-level kinetic model developed by Krippendorff et al. [34]. Currently it is assumed that once internalized each molecule of ADC will release DAR number of payloads instantaneously, however it is well known that depending on the nature of the linker, the intracellular site and time taken for the payload release may vary. In addition, the contribution of endosomal and lysosomal processing in the intracellular payload release is also well appreciated; however a quantitative understanding of these phenomena (especially related to ADC) is scarce. We intend to perform further intracellular trafficking studies to better understand the intracellular fate of ADC and payload, and to obtain relevant parameters, for incorporation into the model. Moreover, we plan to incorporate the intracellular pharmacological interaction between the drug (i.e. released payload) and the target (e.g. microtubulin) to better characterize the Pillar-2.

When it comes to characterizing the PD effect of anticancer drugs most of the available models [7, 17, 31, 32], including the one presented, employ some combination of growth, kill, and transduction sub-models. To develop a more mechanistic model, and integrate cellular biomarkers into the model to address Pillar-3, use of a 'mechanism of action' specific cell cycle model to characterize the PD effect of ADCs is envisioned. We believe that this enhanced mechanistic PD model will not only increase the confidence in drug

development and preclinical-to-clinical translation, but will also help achieve an in vitro in vivo correlation (IVIVC) for ADCs. We have performed kinetic in vitro cell culture experiments (data not published) to analyze the effect of ADC on cell viability and different cellular level biomarkers. Such studies provide information to estimate relevant system and drug specific parameter which can then be incorporated into the PK/PD model to achieve consensus between the in vitro and in vivo system. Of note, the implementation of aforementioned kinetic in vitro experiment and characterization of the data from this experiment may be a much better way of screening/differentiate ADCs at the drug discovery stage compared to the routinely used single time point analysis [31, 35], with the potential of using the in vitro data to establish an IVIVC.

In summary, a mechanistic multi-scale PK/PD platform model has been developed for ADCs, along with a framework for preclinical to clinical translation of their efficacy. The model was successfully able to predict clinical responses for brentuximab-vedotin. Although the proposed model holds promise, a thorough retrospective and prospective evaluation of its ability to predict clinical efficacy of ADCs, based on preclinical data, is warranted.

Acknowledgments The author would like to thank Hugh Barton, Paolo Vicini, Joseph Boni and Jeremy Barton for critical review of this manuscript.

References

1. Webb S (2011) Pharma interest surges in antibody drug conjugates. Nat Biotechnol 29(4):297–298
2. Ducry L, Stump B (2010) Antibody-drug conjugates: linking cytotoxic payloads to monoclonal antibodies. Bioconjug Chem 21(1):5–13
3. Zhou Q, Gallo JM (2011) The pharmacokinetic/pharmacodynamic pipeline: translating anticancer drug pharmacology to the clinic. AAPS J 13(1):111–120
4. Younes A, Yasothan U, Kirkpatrick P (2012) Brentuximab-vedotin. Nat Rev Drug Discov 11(1):19–20
5. Sanderson RJ, Hering MA, James SF, Sun MM, Doronina SO, Siadak AW, Senter PD, Wahl AF (2005) In vivo drug-linker stability of an anti-CD30 dipeptide-linked auristatin immunoconjugate. Clin Cancer Res 11(2 Pt 1):843–852
6. Agoram BM, van der Graaf PH (2012) Biomarkers and biomeasures: key enablers for pharmacokinetic–pharmacodynamic modeling in drug discovery and development. Bioanalysis 4(10):1143–1145
7. Haddish-Berhane N, Shah DK, Betts A, Ma D, DiJoseph J, Leal M, Sapra P, Hans-Peter G (2012) A PK/PD modeling and simulation approach to predict clinical efficacy of antibody drug conjugates from mouse xenograft data. J Pharmacokinet Pharmacodyn (manuscript in preparation)
8. Okeley NM, Miyamoto JB, Zhang X, Sanderson RJ, Benjamin DR, Sievers EL, Senter PD, Alley SC (2010) Intracellular activation of SGN-35, a potent anti-CD30 antibody-drug conjugate. Clin Cancer Res 16(3):888–897
9. Alley SC (2010) Antibody–Auristatin conjugates for cancer: antibody and drug pharmacokinetics and disposition. Paper presented at the AAPS national biotechnology conference, San Francisco, 16 May 2010–19 May 2010
10. Schmidt MM, Wittrup KD (2009) A modeling analysis of the effects of molecular size and binding affinity on tumor targeting. Mol Cancer Ther 8(10):2861–2871
11. Thurber GM, Schmidt MM, Wittrup KD (2008) Antibody tumor penetration: transport opposed by systemic and antigen-mediated clearance. Adv Drug Deliv Rev 60(12):1421–1434
12. Thurber GM, Schmidt MM, Wittrup KD (2008) Factors determining antibody distribution in tumors. Trends Pharmacol Sci 29(2):57–61
13. Hamblett KJ, Senter PD, Chace DF, Sun MM, Lenox J, Cerveny CG, Kissler KM, Bernhardt SX, Kopcha AK, Zabinski RF, Meyer DL, Francisco JA (2004) Effects of drug loading on the antitumor activity of a monoclonal antibody drug conjugate. Clin Cancer Res 10(20):7063–7070
14. Alley S, Kissler K, Morris-Tilden C, Miyamoto J, Senter P, Benjamin D (2007) Effective tumor targeting by auristatin antibody-drug conjugates. AACR meeting abstracts (annual_meeting):# 4088. AACR, Philadelphia
15. Francisco JA, Cerveny CG, Meyer DL, Mixan BJ, Klussman K, Chace DF, Rejniak SX, Gordon KA, DeBlanc R, Toki BE, Law CL, Doronina SO, Siegall CB, Senter PD, Wahl AF (2003) cAC10-vcMMAE, an anti-CD30-monomethyl auristatin E conjugate with potent and selective antitumor activity. Blood 102(4):1458–1465
16. Senter P (2009) Prospects and challenges for antibody targeting: antibody-drug conjugates (ADCs). Paper presented at the European federation for pharmaceutical sciences presentation, Stockholm
17. Simeoni M, Magni P, Cammia C, De Nicolao G, Croci V, Pesenti E, Germani M, Poggesi I, Rocchetti M (2004) Predictive pharmacokinetic–pharmacodynamic modeling of tumor growth kinetics in xenograft models after administration of anticancer agents. Cancer Res 64(3):1094–1101
18. Yang J, Mager DE, Straubinger RM (2010) Comparison of two pharmacodynamic transduction models for the analysis of tumor therapeutic responses in model systems. AAPS J 12(1):1–10
19. Younes A, Bartlett NL, Leonard JP, Kennedy DA, Lynch CM, Sievers EL, Forero-Torres A (2010) Brentuximab-vedotin (SGN-35) for relapsed CD30-positive lymphomas. N Engl J Med 363(19):1812–1821
20. Bartlett NL, Forero-Torres A, Rosenblatt JD, Fanale M, Horning SJ, Thompson S, Sievers EL, Kennedy DA (2009) Complete remissions with SGN-35 weekly dosing: a phase 1 dose-escalation study in relapsed/refractory HL or systemic ALCL patients. Paper presented at the ASCO annual meeting, Orlando, 29 May 2009–6 June 2009
21. Fromm JR, McEarchern JA, Kennedy D, T. A, Shustov AR, Gopal AK (2010: # 1789) Preclinical and clinical binding properties, internalization kinetics, and clinicopathological activity of brentuximab-vedotin (SGN-35): a novel antibody drug conjugate for anaplastic large cell lymphoma and classical Hodgkin lymphoma. Paper presented at the American society of hematology 2010 annual meeting, Orlando, 12 April 2010–12 July 2010
22. Brons PP, Raemaekers JM, Bogman MJ, van Erp PE, Boezeman JB, Pennings AH, Wessels HM, Haanen C (1992) Cell cycle kinetics in malignant lymphoma studied with in vivo iododeoxyuridine administration, nuclear Ki-67 staining, and flow cytometry. Blood 80(9):2336–2343
23. Zhao Y, Kosorok MR, Zeng D (2009) Reinforcement learning design for cancer clinical trials. Stat Med 28(26):3294–3315
24. Fanale MA, Forero-Torres A, Rosenblatt JD, Advani RH, Franklin AR, Kennedy DA, Han TH, Sievers EL, Bartlett NL

(2012) A phase I weekly dosing study of brentuximab-vedotin in patients with relapsed/refractory CD30-positive hematologic malignancies. Clin Cancer Res 18(1):248–255
25. Cheson BD, Pfistner B, Juweid ME, Gascoyne RD, Specht L, Horning SJ, Coiffier B, Fisher RI, Hagenbeek A, Zucca E, Rosen ST, Stroobants S, Lister TA, Hoppe RT, Dreyling M, Tobinai K, Vose JM, Connors JM, Federico M, Diehl V (2007) Revised response criteria for malignant lymphoma. J Clin Oncol 25(5):579–586
26. D'Argenio DZ, Schumitzky A (1979) A program package for simulation and parameter estimation in pharmacokinetic systems. Comput Programs Biomed 9(2):115–134
27. Arrowsmith J (2011) Trial watch: phase II failures: 2008–2010. Nat Rev Drug Discov 10(5):328–329
28. Berry DA (2011) Adaptive clinical trials in oncology. Nat Rev Clin Oncol 9(4):199–207
29. Begley CG, Ellis LM (2012) Drug development: raise standards for preclinical cancer research. Nature 483:531–533
30. Ternant D, Henin E, Cartron G, Tod M, Paintaud G, Girard P (2009) Development of a drug-disease simulation model for rituximab in follicular non-Hodgkin's lymphoma. Br J Clin Pharmacol 68(4):561–573
31. Lobo ED, Balthasar JP (2002) Pharmacodynamic modeling of chemotherapeutic effects: application of a transit compartment model to characterize methotrexate effects in vitro. AAPS Pharm Sci 4(4):E42
32. Jumbe NL, Xin Y, Leipold DD, Crocker L, Dugger D, Mai E, Sliwkowski MX, Fielder PJ, Tibbitts J (2010) Modeling the efficacy of trastuzumab-DM1, an antibody drug conjugate, in mice. J Pharmacokinet Pharmacodyn 37(3):221–242
33. Morgan P, Van Der Graaf PH, Arrowsmith J, Feltner DE, Drummond KS, Wegner CD, Street SD (2012) Can the flow of medicines be improved? Fundamental pharmacokinetic and pharmacological principles toward improving phase II survival. Drug Discov Today 17(9–10):419–424
34. Krippendorff BF, Oyarzun DA, Huisinga W (2012) Predicting the F(ab)-mediated effect of monoclonal antibodies in vivo by combining cell-level kinetic and pharmacokinetic modelling. J Pharmacokinet Pharmacodyn 39(2):125–139
35. Wang X, Ma D, Olson WC, Heston WD (2011) In vitro and in vivo responses of advanced prostate tumors to PSMA ADC, an auristatin-conjugated antibody to prostate-specific membrane antigen. Mol Cancer Ther 10(9):1728–1739
36. Nagata S, Onda M, Numata Y, Santora K, Beers R, Kreitman RJ, Pastan I (2002) Novel anti-CD30 recombinant immunotoxins containing disulfide-stabilized Fv fragments. Clin Cancer Res 8(7):2345–2355
37. Sutherland MS, Sanderson RJ, Gordon KA, Andreyka J, Cerveny CG, Yu C, Lewis TS, Meyer DL, Zabinski RF, Doronina SO, Senter PD, Law CL, Wahl AF (2006) Lysosomal trafficking and cysteine protease metabolism confer target-specific cytotoxicity by peptide-linked anti-CD30-auristatin conjugates. J Biol Chem 281(15):10540–10547